Available online at www.sciencedirect.com
ScienceDirect
International Journal of Thermal Sciences 46 (2007) 998–1010
International Journal of Thermal Sciences
www.elsevier.com/locate/ijts

Prediction of temperature distribution and Nusselt number in rectangular microchannels at wall slip condition for all versions of constant wall temperature

Lütfullah Kuddusi *

Istanbul Technical University, Faculty of Mechanical Engineering, Mechanical Engineering Department, Gümüşsuyu, 34437 Istanbul, Turkey

Received 24 May 2006; received in revised form 8 December 2006; accepted 14 December 2006

Available online 2 February 2007

Abstract

Slip flow in rectangular microchannels heated at constant and uniform wall temperature (H1 boundary condition) is studied. The study is extended to the eight possible thermal versions that are formed of different combinations of heated and adiabatic walls. Integral transform method is applied to derive the velocity and temperature distributions and thus, the average Nusselt number for all the eight thermal versions. It is found that, for microchannels with perfect accommodation for velocity and temperature, the rarefaction has a decreasing effect on heat transfer for all the eight thermal versions. The results of the paper for the special case of non-slip flow agree exactly with the results found for macrochannels in literature.

Keywords: Slip-flow; Microchannel; Heat transfer; Nusselt number; Knudsen number

1. Introduction

Slip flow occurs if the flow pressure is very low or the characteristic size of the flow system is small. Continuum physics is no longer valid if the characteristic size of the flow system is comparable to the molecular mean free path. In non-slip flow, as a requirement of continuum physics, the flow velocity is zero at fluid-solid interface and the fluid temperature at the vicinity of solid walls is equal to that of the solid walls. In the presence of slip flow, the flow velocity at the solid walls is nonzero and there is a temperature jump (a finite difference between the temperatures of solid wall and the fluid at the vicinity of solid wall). Nonzero flow velocity and temperature jump at the solid walls are major hydrodynamic and thermal effects that should be taken into account in the slip flow solutions.

Slip flow solutions in microchannels may be investigated for two cases; when the walls of the microchannel are heated at constant and uniform temperature (H1 boundary condition) and; when the walls of the microchannel are heated at constant and uniform heat flux (H2 boundary condition). In literature, each of these cases is divided into eight sub versions that are formed of different combinations of heated and adiabatic walls.

Morini [1] and Spiga and Morini [2] have solved the flow in macrochannels for all the eight thermal versions under H1 and H2 boundary conditions, respectively. Tunc and Bayazitoglu [3] have solved the slip flow in microchannels under H2 boundary condition for the specific case when all the walls of microchannel are heated at constant and uniform heat flux. They determined the Nusselt number for various rarefaction intensities and microchannel aspect ratios, and found that rarefaction has a decreasing effect on the heat transfer. Ghodoossi and Egrican [4] solved the slip flow in microchannels under H1 boundary condition for the specific case when all the walls of microchannel are heated at constant and uniform temperature. Similar heat transfer behaviors are reported as those in the work of Tunc and Bayazitoglu [3].

In this paper, the slip flow in microchannels under H1 boundary condition is studied for all the eight thermal versions. Temperature distribution and Nusselt number for all of the eight thermal versions are determined. The results for the special case

* Tel.: +90 212 2931300 (2452); fax: +90 212 2450795.
E-mail address: kuddusi@itu.edu.tr.

1290-0729/$ – see front matter
doi:10.1016/j.ijthermalsci.2006.12.006

Nomenclature

a	long side of microchannel	m
A_n	constant defined by Eq. (25)	
b	short side of microchannel	m
$b_{1,n}, b_{2,n}, b_{3,n}$	constants defined by Eqs. (30)–(32)	
B_n	constant defined by Eq. (33)	
$c_{i,j}$	constant coefficients in Eqs. (93)–(100)	
c_P	specific heat	$\mathrm{J\,kg^{-1}\,K^{-1}}$
$C_{1n} \cdots C_{4n}$	constants defined by Eqs. (86)–(89)	
C_{3mn}, C_{4mn}	constants defined by Eqs. (90) and (91)	
$d_1 \cdots d_{12}$	constants equal to 1 or 0	
D_h	hydraulic diameter	m
h	convection heat transfer coefficient	$\mathrm{W\,m^{-2}\,K^{-1}}$
I_{mn}	constant defined by Eq. (92)	
k	thermal conductivity	$\mathrm{W\,m^{-1}\,K^{-1}}$
K	Kernel	
Kn	Knudsen number	
L_h	heated perimeter of microchannel	m
$\hat{L}_h$	nondimensional heated perimeter of microchannel	
Nu	Nusselt number	
p	fluid pressure	Pa
P	normalized pressure gradient	
Pr	Prandtl number	
q'	thermal power per unit length of microchannel	$\mathrm{W\,m^{-1}}$
R	specific heat ratio	
S_1, S_2, S_3, S_4	constants introduced for simplicity defined by Eqs. (41)–(44)	
T	temperature	K
$\widehat{T}$	nondimensional temperature	
$\widehat{T}_{\mathrm{aux}}$	auxiliary function	
u	fluid velocity	$\mathrm{m\,s^{-1}}$
$\widehat{u}$	nondimensional fluid velocity	
v	dependent variable defined by Eq. (12)	
$\bar{v}$	transformed dependent variable defined by Eq. (19)	
x, y, z	nondimensional coordinates	

Greek symbols

α	thermal diffusivity	$\mathrm{m^2\,s^{-1}}$
γ	aspect ratio	
λ_n	eigenvalues for the energy equation	
λ_{mfp}	molecular mean free path	m
μ	dynamic viscosity	$\mathrm{kg\,m^{-1}\,s^{-1}}$
μ_n	eigenvalues for the momentum equation	
ρ	density	$\mathrm{kg\,m^{-3}}$
θ	dependent variable defined by Eqs. (65) and (66)	
$\bar{\theta}$	transformed dependent variable defined by Eqs. (78) and (80)	
ξ, η, ζ	coordinates	m

Subscripts

b	bulk property
m	mean value
n	index
s	fluid property near the wall
w	wall value
0	inlet property

of zero rarefaction (solution for macrochannel) agree exactly with the results of Morini [1] who solved the macrochannel flow for the same eight thermal versions. One of the eight thermal versions, microchannel with four heated walls, is solved by Yu and Ameel [5] for thermally developing flow at slip condition, the result of which is given graphically in the form of both local and fully developed mean Nusselt numbers. The fully developed Nusselt numbers found for the mentioned thermal version agree with those of Yu and Ameel [5].

2. Problem statement

The problem under consideration is a hydrodynamically and thermally developed steady flow in the rectangular microchannel shown in Fig. 1. It is supposed that the dimensions of the microchannel are comparable to the molecular mean free path. According to the explanations above, a slip flow will occur in the microchannel. That is, a nonzero flow velocity and a temperature jump will occur at the walls of microchannel. The properties of such a slip flow are quantified by the Knudsen number Kn, which is defined as the ratio of the molecular mean free path to the characteristic length of microchannel. According to Beskok and Karniadakis [6], non-slip flow (flow in macrochannels) occurs if the Knudsen number is lower than 0.001 and, slip flow (flow in microchannels) occurs if the Knudsen number ranges from 0.001 to 0.1. The range of interest in this paper for Knudsen number is from 0.001 to 0.1.

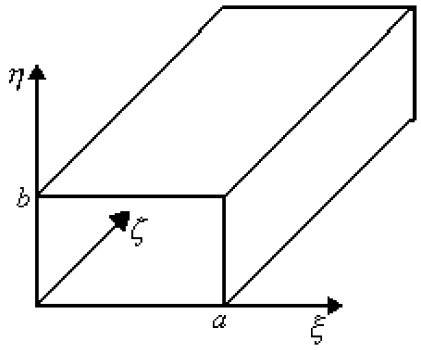

Fig. 1. The geometry of microchannel.

If the problem under consideration was a non-slip flow, the temperature of the flow near the wall, T_s, would be equal to the wall temperature, T_w, and the velocity of the flow near the wall, u_s, would be equal to zero. Since the problem under consideration is a slip flow, the temperature of the flow near the wall is no longer equal to the wall temperature and the velocity of the flow near the wall is no longer zero. The temperature and velocity of the flow at the bottom wall are given by Barron et al. [7], as

$$T_s = T_w + \frac{2R}{1+R}\frac{\lambda_{\mathrm{mfp}}}{Pr}\left.\frac{\partial T}{\partial \eta}\right|_{\eta=0} \tag{1}$$

$$u_s = \lambda_{\mathrm{mfp}}\left.\frac{\partial u}{\partial \eta}\right|_{\eta=0} \tag{2}$$

The relations above are used to calculate local temperature jump and slip velocity at solid walls. The local values averaged over the heated perimeter of the microchannel are then used in Nusselt number calculation. Since the study mainly aims to investigate the effect of different thermal versions, the tangential momentum accommodation coefficient and the thermal accommodation coefficient are not included in the equations above. In any case, for most engineering applications, values for the accommodation coefficients are near unity.

The flow is governed by the Navier–Stokes equations if the continuum condition (very low Knudsen number, $Kn < 0.001$) is satisfied. The continuum form of flow does not exist in a microchannel under slip flow. Therefore the slip flow solution by using the Navier–Stokes equations may result in no negligible deviations in the hydrodynamic and thermal properties of the flow. However, the general belief of the investigators is that the Navier–Stokes equations may be used for slip flow solution with high accuracy provided the boundary conditions are modified according to the slip flow characteristics. Modification of the boundary conditions (nonzero flow velocity and temperature jump at the boundaries) removes the error raised by not properly usage of the Navier–Stokes equations in slip flow solution.

The H1 boundary condition can be applied to a rectangular microchannel in eight different versions that are obtained by different combinations of heated (at constant temperature) and adiabatic walls. In Refs. [1,2], these versions are given as

4 version: Four walls are heated.
3L version: Three walls are heated, one short wall is adiabatic.
3S version: Three walls are heated, one long wall is adiabatic.
2L version: Two walls are heated, two short walls are adiabatic.
2S version: Two walls are heated, two long walls are adiabatic.
2C version: One short and one long wall are heated, the other two walls are adiabatic.
1L version: One long wall is heated, the other three walls are adiabatic.
1S version: One short wall is heated, the other three walls are adiabatic.

The slip flow in a microchannel with eight different H1 thermal versions above will be solved by applying the Navier–Stokes equations and modified boundary conditions.

3. Momentum equation

The ζ-direction momentum equation for a hydrodynamically developed flow is

$$\frac{\partial^2 u}{\partial \xi^2} + \frac{\partial^2 u}{\partial \eta^2} = \frac{1}{\mu}\frac{\partial p}{\partial \zeta} \tag{3}$$

The modified hydrodynamic boundary conditions according to the slip flow assumption are

$$u = u_s \quad \text{at } \xi = 0,\ \xi = a,\ \eta = 0,\ \eta = b \tag{4}$$

The momentum equation and the modified boundary conditions are nondimensionalized by introducing the following nondimensional variables

$$x = \frac{\xi}{a}, \quad 0 \leqslant x \leqslant 1, \tag{5}$$

$$y = \frac{\eta}{a}, \quad 0 \leqslant y \leqslant \gamma \equiv \frac{b}{a} \tag{6}$$

$$\widehat{u}(x, y) = \frac{u(\xi, \eta)}{u_m} \tag{7}$$

where u_m represents the mean fluid velocity, which is defined as

$$u_m = \frac{1}{ab}\int_0^b \int_0^a u(\xi, \eta)\, d\xi\, d\eta \tag{8}$$

The nondimensional momentum equation and associated boundary conditions are found as

$$\frac{\partial^2 \widehat{u}}{\partial x^2} + \frac{\partial^2 \widehat{u}}{\partial y^2} = P \tag{9}$$

$$\widehat{u} = \widehat{u}_s \quad \text{at } x = 0,\ x = 1,\ y = 0,\ y = \gamma \tag{10}$$

where the normalized pressure gradient P is defined as

$$P = \frac{a^2}{u_m \mu}\frac{\partial p}{\partial \zeta} \tag{11}$$

The nondimensional momentum equation contains four nonhomogeneous boundary conditions. The nonhomogeneous boundary conditions in y-direction are homogenized by means of a change of dependent variable defined as

$$v(x, y) = \widehat{u}(x, y) - \widehat{u}_y(y) \tag{12}$$

where the auxiliary one direction $\widehat{u}_y(y)$ function satisfies the following differential equation and the same boundary conditions for the nondimensional momentum equation at $y = 0$ and $y = \gamma$

$$\frac{d^2 \widehat{u}_y}{dy^2} - \widehat{u}_y = 0 \tag{13}$$

$$\widehat{u}_y = \widehat{u}_s \quad \text{at } y = 0,\ y = \gamma \tag{14}$$

The solution of system above is found as

$$\widehat{u}_y = \frac{\widehat{u}_s}{1 + e^{\gamma}}\left(e^{y} + e^{\gamma - y}\right) \tag{15}$$

By applying the change of dependent variable as defined above the governing nondimensional momentum equation and associated boundary conditions take the following form.

$$\frac{\partial^2 v}{\partial x^2} + \frac{\partial^2 v}{\partial y^2} = P - \frac{\widehat{u}_s}{1 + e^{\gamma}}\left(e^{y} + e^{\gamma - y}\right) \tag{16}$$

$$v = \widehat{u}_s - \widehat{u}_y \quad \text{at } x = 0,\ x = 1 \tag{17}$$

$$v = 0 \quad \text{at } y = 0,\ y = \gamma \tag{18}$$

The system above will be solved by applying integral transform method. Application of integral transform together with homogenized boundary conditions will reduce the two-dimensional momentum equation above to a one-dimensional (ordinary) differential equation the solution of which may easily be obtained.

4. Solution of the momentum equation

The integral transform and inversion formula to be used are Integral transform

$$\bar{v}(\mu_n, x) = \int_0^\gamma K(\mu_n, y) v(x, y)\, dy \tag{19}$$

Inversion formula

$$v(x, y) = \sum_{n=1}^{\infty} K(\mu_n, y)\bar{v}(\mu_n, x) \tag{20}$$

where the Kernels $K(\mu_n, y)$ and the eigenvalues μ_n are the same as those used in heat conduction problems. Ozisik [8] proposes the following Kernels and eigenvalues for the boundary conditions of the first kind both at $y = 0$ and $y = \gamma$ in the solution of heat conduction problems by integral transform method.

$$K(\mu_n, y) = \sqrt{\frac{2}{\gamma}} \sin \mu_n y \tag{21}$$

$$\sin \mu_n \gamma = 0, \quad \text{or,} \quad \mu_n = \frac{n\pi}{\gamma} \quad n = 1, 2, 3, \ldots \tag{22}$$

Interested readers may refer to the books [9–12] for details on the application of integral transforms in solution of heat and fluid flow problems. We will start the transformation by multiplying both sides of the nondimensional momentum equation (Eq. (16)) by $K(\mu_n, y)$ and integrating over the y axis,

$$\int_0^\gamma K(\mu_n, y)\frac{\partial^2 v}{\partial x^2}\, dy + \int_0^\gamma K(\mu_n, y)\frac{\partial^2 v}{\partial y^2}\, dy = \int_0^\gamma K(\mu_n, y) P\, dy - \int_0^\gamma K(\mu_n, y)\frac{\widehat{u}_s}{1 + e^\gamma}\left(e^y + e^{\gamma - y}\right) dy \tag{23}$$

Evaluation of the four integrals changes this equation to

$$\frac{\partial^2 \bar{v}(\mu_n, x)}{\partial x^2} - \mu_n^2 \bar{v}(\mu_n, x) = A_n \tag{24}$$

where

$$A_n = \sqrt{\frac{2}{\gamma}}\frac{E_n}{\mu_n}\left(P - \frac{\widehat{u}_s \mu_n^2}{1 + \mu_n^2}\right) \tag{25}$$

$$E_n = -(-1)^n + 1 \tag{26}$$

The boundary conditions at $x = 0$ and $x = 1$ are also transformed as

$$\bar{v}(\mu_n, 0) = \int_0^\gamma K(\mu_n, y) v(0, y)\, dy = \sqrt{\frac{2}{\gamma}}\frac{\widehat{u}_s E_n}{\mu_n(1 + \mu_n^2)} \tag{27}$$

$$\bar{v}(\mu_n, 1) = \int_0^\gamma K(\mu_n, y) v(1, y)\, dy = \sqrt{\frac{2}{\gamma}}\frac{\widehat{u}_s E_n}{\mu_n(1 + \mu_n^2)} \tag{28}$$

The transformed form of the momentum equation, Eq. (24), is an ordinary differential equation the solution of which according to the boundary conditions, Eqs. (27) and (28), is

$$\bar{v}(\mu_n, x) = b_{1,n} e^{\mu_n x} + b_{2,n} e^{-\mu_n x} - b_{3,n} \tag{29}$$

where

$$b_{1,n} = B_n \frac{-e^{-\mu_n} + 1}{e^{\mu_n} - e^{-\mu_n}} \tag{30}$$

$$b_{2,n} = B_n \frac{e^{\mu_n} - 1}{e^{\mu_n} - e^{-\mu_n}} \tag{31}$$

$$b_{3,n} = \frac{A_n}{\mu_n^2} \tag{32}$$

$$B_n = \sqrt{\frac{2}{\gamma}}\frac{P E_n}{\mu_n^3} \tag{33}$$

Applying the inversion formula results in

$$v(x, y) = \sum_{n=1}^{\infty} K(\mu_n, y)\left(b_{1,n} e^{\mu_n x} + b_{2,n} e^{-\mu_n x} - b_{3,n}\right) \tag{34}$$

Finally, the nondimensional velocity distribution is found by substituting Eqs. (15) and (34) into Eq. (12) as

$$\widehat{u}(x, y) = \frac{\widehat{u}_s}{1 + e^\gamma}\left(e^y + e^{\gamma - y}\right) + \sum_{n=1}^{\infty} K(\mu_n, y)\left(b_{1,n} e^{\mu_n x} + b_{2,n} e^{-\mu_n x} - b_{3,n}\right) \tag{35}$$

The velocity distribution found above provides a possibility to determine the nondimensional slip velocity $\widehat{u}_s$ and the normalized pressure gradient P, which are still unknowns.

Eqs. (2) and (8) may be written in terms of nondimensional variables, respectively, as

$$\widehat{u}_s = Kn \left.\frac{\partial \widehat{u}(x, y)}{\partial y}\right|_{y=0} \tag{36}$$

$$1 = \frac{1}{\gamma}\int_0^\gamma \int_0^1 \widehat{u}(x, y)\, dx\, dy \tag{37}$$

where the Knudsen number Kn is defined as

$$Kn = \frac{\lambda_{\text{mfp}}}{D_h} \tag{38}$$

Importing Eq. (35) into Eqs. (36) and (37) and solving simultaneously for the nondimensional slip velocity $\widehat{u}_s$ and the normalized pressure gradient P result in

$$\widehat{u}_s = \frac{S_3}{S_1}\frac{\gamma}{2\left[\frac{1+\gamma}{2\gamma Kn} - \frac{1-e^\gamma}{1+e^\gamma}\left(1 + \frac{S_3}{S_1}\right) - \frac{4}{\gamma}S_2\left(\frac{S_4}{S_2} - \frac{S_3}{S_1}\right)\right]} \tag{39}$$

$$P = \frac{1}{8S_1}\left\{\gamma^2 - \widehat{u}_s\left[\frac{2(e^\gamma - 1)\gamma}{1 + e^\gamma} + 8S_2\right]\right\} \tag{40}$$

where

$$S_1 = \sum_{n=1}^{\infty} \frac{2\tanh \mu_{2n-1}/2 - \mu_{2n-1}}{\mu_{2n-1}^5} \tag{41}$$

$$S_2 = \sum_{n=1}^{\infty} \frac{1}{\mu_{2n-1}^2(1+\mu_{2n-1}^2)} \tag{42}$$

$$S_3 = \sum_{n=1}^{\infty} \frac{2\tanh \mu_{2n-1}/2 - \mu_{2n-1}}{\mu_{2n-1}^3} \tag{43}$$

$$S_4 = \sum_{n=1}^{\infty} \frac{1}{1+\mu_{2n-1}^2} \tag{44}$$

Note that Eq. (36) gives the local nondimensional slip velocity along the long wall of microchannel. The nondimensional slip velocity $\widehat{u}_s$ found above is the average of local values along the long wall. Determination of the nondimensional slip velocity $\widehat{u}_s$ and the normalized pressure gradient P completes the solution of momentum equation.

The velocity distribution given by Eq. (35), which is obtained by applying the integral transform in y-direction, will be employed in derivation of temperature distribution. However, for some of the eight thermal versions, employing the velocity distribution obtained by applying the integral transform in x-direction will highly simplify the mathematical process in derivation of the temperature distribution.

By applying the integral transform in x-direction with homogenized boundary conditions in the same direction, the velocity distribution is obtained as

$$\widehat{u}(x,y) = \frac{\widehat{u}_s}{1+e}\left(e^x + e^{1-x}\right) + \sum_{n=1}^{\infty} K(\mu_n, x)\left(b_{1,n}e^{\mu_n y} + b_{2,n}e^{-\mu_n y} - b_{3,n}\right) \tag{45}$$

where

$$K(\mu_n, x) = \sqrt{2}\sin \mu_n x \tag{46}$$

$$\sin \mu_n = 0, \quad \text{or,} \quad \mu_n = n\pi \quad n = 1, 2, 3, \ldots \tag{47}$$

$$A_n = \sqrt{2}\frac{E_n}{\mu_n}\left(P - \frac{\widehat{u}_s \mu_n^2}{1+\mu_n^2}\right) \tag{48}$$

$$B_n = \sqrt{2}\frac{P E_n}{\mu_n^3} \tag{49}$$

$$b_{1,n} = B_n \frac{-e^{-\mu_n \gamma} + 1}{e^{\mu_n \gamma} - e^{-\mu_n \gamma}} \tag{50}$$

$$b_{2,n} = B_n \frac{e^{\mu_n \gamma} - 1}{e^{\mu_n \gamma} - e^{-\mu_n \gamma}} \tag{51}$$

$$b_{3,n} = \frac{A_n}{\mu_n^2} \tag{52}$$

5. Energy equation

The energy equation for a thermally developed flow is

$$\frac{\partial^2 T}{\partial \xi^2} + \frac{\partial^2 T}{\partial \eta^2} = \frac{u(\xi,\eta)}{\alpha}\frac{\partial T}{\partial \zeta} \tag{53}$$

The axial variation of fluid temperature is approximated in the following form by providing an energy balance for an arbitrary differential $d\zeta$ segment of the microchannel.

$$\frac{\partial T}{\partial \zeta} = \frac{q'}{\rho c_P u_m a b} \tag{54}$$

where q' represents the thermal power per unit length imposed on the heated walls of the microchannel.

The energy equation is nondimensionalized by making use of the nondimensional variables defined by Eqs. (5)–(7) and the nondimensional temperature defined as

$$\widehat{T} = \frac{T - T_0}{(q'/k)} \tag{55}$$

The nondimensional energy equation is found as

$$\frac{\partial^2 \widehat{T}}{\partial x^2} + \frac{\partial^2 \widehat{T}}{\partial y^2} = \frac{\widehat{u}(x,y)}{\gamma} \tag{56}$$

6. Thermal boundary conditions

The walls of the microchannel are either adiabatic or heated at a constant temperature T_w. Since the problem under consideration is a slip flow, this statement may be written more precisely as; for the fluid at the vicinity of solid walls, either the temperature gradient is zero, or, the temperature is equal to slip temperature T_s that has a finite difference with the wall temperature T_w. Combinations of the adiabatic and heated walls form the eight versions of the thermal boundary conditions. The thermal boundary conditions for any version may be given in the following form in general. The coefficients d_i equal 1 for non-adiabatic walls and 0 for adiabatic walls. Various combinations of these numerical values associated with each of the eight thermal versions are given in Table 1.

$$\left[d_1 T(\xi,\eta) + d_2 \frac{\partial T(\xi,\eta)}{\partial \xi}\right]_{\xi=0} = d_3 T_s \tag{57}$$

$$\left[d_4 T(\xi,\eta) + d_5 \frac{\partial T(\xi,\eta)}{\partial \xi}\right]_{\xi=a} = d_6 T_s \tag{58}$$

$$\left[d_7 T(\xi,\eta) + d_8 \frac{\partial T(\xi,\eta)}{\partial \eta}\right]_{\eta=0} = d_9 T_s \tag{59}$$

$$\left[d_{10} T(\xi,\eta) + d_{11} \frac{\partial T(\xi,\eta)}{\partial \eta}\right]_{\eta=b} = d_{12} T_s \tag{60}$$

Table 1
Numeric values of the coefficients d_i for determining the thermal boundary conditions in various combinations of heated and adiabatic walls

Version	d_1	d_2	d_3	d_4	d_5	d_6	d_7	d_8	d_9	d_{10}	d_{11}	d_{12}
1L	0	1	0	0	1	0	1	0	1	0	1	0
1S	1	0	1	0	1	0	0	1	0	0	1	0
2L	0	1	0	0	1	0	1	0	1	1	0	1
2S	1	0	1	1	0	1	0	1	0	0	1	0
2C	1	0	1	0	1	0	1	0	1	0	1	0
3L	1	0	1	0	1	0	1	0	1	1	0	1
3S	1	0	1	1	0	1	1	0	1	0	1	0
4	1	0	1	1	0	1	1	0	1	1	0	1

The general form of the thermal boundary conditions may be nondimensionalized as

$$\left[d_1\widehat{T}(x,y)+d_2\frac{\partial\widehat{T}(x,y)}{\partial x}\right]_{x=0}=d_3\widehat{T}_s \tag{61}$$

$$\left[d_4\widehat{T}(x,y)+d_5\frac{\partial\widehat{T}(x,y)}{\partial x}\right]_{x=1}=d_6\widehat{T}_s \tag{62}$$

$$\left[d_7\widehat{T}(x,y)+d_8\frac{\partial\widehat{T}(x,y)}{\partial y}\right]_{y=0}=d_9\widehat{T}_s \tag{63}$$

$$\left[d_{10}\widehat{T}(x,y)+d_{11}\frac{\partial\widehat{T}(x,y)}{\partial y}\right]_{y=\gamma}=d_{12}\widehat{T}_s \tag{64}$$

7. Solution of the energy equation

Some of the thermal boundary conditions (at least one) for any of the eight versions are nonhomogeneous. The nonhomogeneous boundary conditions in the x or y directions are homogenized by means of a change of dependent variable defined, respectively, as

$$\theta(x,y)=\widehat{T}(x,y)-\widehat{T}_x(x) \tag{65}$$

$$\theta(x,y)=\widehat{T}(x,y)-\widehat{T}_y(y) \tag{66}$$

where the auxiliary one direction $\widehat{T}_x(x)$ and $\widehat{T}_y(y)$ functions satisfy the following differential equations and the same boundary conditions at $x=0$, $x=1$ (Eqs. (61) and (62)) and $y=0$, $y=\gamma$ (Eqs. (63) and (64)), respectively.

$$\frac{d^2\widehat{T}_x}{dx^2}-\widehat{T}_x=0 \tag{67}$$

$$\frac{d^2\widehat{T}_y}{dy^2}-\widehat{T}_y=0 \tag{68}$$

In this paper, the nonhomogeneity is removed in x direction for the 1S, 2S and 3S versions and in y direction for the others. According to this solution policy, the auxiliary functions are determined as

$$\widehat{T}_x=\frac{\widehat{T}_s}{e+e^{-1}}\left(e^{x-1}+e^{1-x}\right)\quad\text{for 1S version} \tag{69}$$

$$\widehat{T}_x=\frac{\widehat{T}_s}{1+e}\left(e^{x}+e^{1-x}\right)\quad\text{for 2S and 3S versions} \tag{70}$$

$$\widehat{T}_y=\frac{\widehat{T}_s}{e^{\gamma}+e^{-\gamma}}\left(e^{y-\gamma}+e^{\gamma-y}\right)\quad\text{for 1L and 2C versions} \tag{71}$$

$$\widehat{T}_y=\frac{\widehat{T}_s}{1+e^{\gamma}}\left(e^{y}+e^{\gamma-y}\right)\quad\text{for 4, 2L and 3L versions} \tag{72}$$

By applying the change of dependent variable as defined above the nondimensional energy equation (Eq. (56)) and associated boundary conditions (Eqs. (61)–(64)) take the following form, respectively.

$$\frac{\partial^2\theta}{\partial x^2}+\frac{\partial^2\theta}{\partial y^2}=\frac{\widehat{u}(x,y)}{\gamma}-\widehat{T}_{\text{aux}} \tag{73}$$

$$\left[d_1\theta(x,y)+d_2\frac{\partial\theta(x,y)}{\partial x}\right]_{x=0}=d_3\widehat{T}_s-\left[d_1\widehat{T}_{\text{aux}}+d_2\frac{d\widehat{T}_{\text{aux}}}{dx}\right]_{x=0} \tag{74}$$

$$\left[d_4\theta(x,y)+d_5\frac{\partial\theta(x,y)}{\partial x}\right]_{x=1}=d_6\widehat{T}_s-\left[d_4\widehat{T}_{\text{aux}}+d_5\frac{d\widehat{T}_{\text{aux}}}{dx}\right]_{x=1} \tag{75}$$

$$\left[d_7\theta(x,y)+d_8\frac{\partial\theta(x,y)}{\partial y}\right]_{y=0}=d_9\widehat{T}_s-\left[d_7\widehat{T}_{\text{aux}}+d_8\frac{d\widehat{T}_{\text{aux}}}{dy}\right]_{y=0} \tag{76}$$

$$\left[d_{10}\theta(x,y)+d_{11}\frac{\partial\theta(x,y)}{\partial y}\right]_{y=\gamma}=d_{12}\widehat{T}_s-\left[d_{10}\widehat{T}_{\text{aux}}+d_{11}\frac{d\widehat{T}_{\text{aux}}}{dy}\right]_{y=\gamma} \tag{77}$$

where the auxiliary function $\widehat{T}_{\text{aux}}$ is given by either of the Eqs. (69)–(72), depending on the thermal version being solved. It is notable that the right sides of the homogenized boundary conditions given above vanish either in x or in y direction. That is, the boundary conditions either in x or in y direction are homogeneous. The right sides of Eqs. (74) and (75) are equal to zero for the 1S, 2S and 3S versions, and the right sides of the Eqs. (76) and (77) are equal to zero for all the other versions.

The solution of energy equation coupled with the boundary conditions given above is sought.

Integral transform method, either in x or in y direction, is applied to solve the energy equation. The integral transform and inversion formula in x and y directions to be used in the solution of energy equation are:

Integral transform (in x direction)

$$\bar{\theta}(\lambda_n,y)=\int_0^1 K(\lambda_n,x)\theta(x,y)\,dx \tag{78}$$

Inversion formula (in x direction)

$$\theta(x,y)=\sum_{n=1}^{\infty}K(\lambda_n,x)\bar{\theta}(\lambda_n,y) \tag{79}$$

Integral transform (in y direction)

$$\bar{\theta}(\lambda_n,x)=\int_0^{\gamma} K(\lambda_n,y)\theta(x,y)\,dy \tag{80}$$

Inversion formula (in y direction)

$$\theta(x,y)=\sum_{n=1}^{\infty}K(\lambda_n,y)\bar{\theta}(\lambda_n,x) \tag{81}$$

where the Kernels $K(\lambda_n,x)$, $K(\lambda_n,y)$ and the eigenvalues λ_n are the same as those used in heat conduction problems. These are determined according to the combination of the boundary

Table 2
The Kernels and the eigenvalues used in transformation of the energy equation for the eight thermal versions

Version	$K(\lambda_n, x)$	$K(\lambda_n, y)$	λ_n
1L	–	$\sqrt{2/\gamma}\sin\lambda_n y$	$(2n-1)\pi/(2\gamma)$
1S	$\sqrt{2}\sin\lambda_n x$	–	$(2n-1)\pi/2$
2L	–	$\sqrt{2/\gamma}\sin\lambda_n y$	$n\pi/\gamma$
2S	$\sqrt{2}\sin\lambda_n x$	–	$n\pi$
2C	–	$\sqrt{2/\gamma}\sin\lambda_n y$	$(2n-1)\pi/(2\gamma)$
3L	–	$\sqrt{2/\gamma}\sin\lambda_n y$	$n\pi/\gamma$
3S	$\sqrt{2}\sin\lambda_n x$	–	$n\pi$
4	–	$\sqrt{2/\gamma}\sin\lambda_n y$	$n\pi/\gamma$

$n = 1, 2, 3, \ldots$

conditions in the transformation direction. Ozisik [8] has tabulated the Kernels and eigenvalues for all possible combinations of the homogeneous boundary conditions of the first kind (zero temperature at the boundary) and second kind (adiabatic boundary). The Kernels and the eigenvalues to be used for the eight thermal versions, proposed by Ozisik [8], are given in Table 2.

Similar to the case of momentum equation, the transformation starts by multiplying both sides of the nondimensional energy equation (Eq. (73)) by $K(\lambda_n, x)$ or $K(\lambda_n, y)$ and integrating over the x or y axis. The transformation results in a second order ordinary differential equation with a single space variable for each of the thermal versions as

$$\frac{\partial^2\bar{\theta}(\lambda_n, y)}{\partial y^2} - \lambda_n^2\bar{\theta}(\lambda_n, y) = C_{1n} + \frac{1}{\gamma}\left(b_{1,n}e^{\mu_n y} + b_{2,n}e^{-\mu_n y}\right)$$

for 2S and 3S versions (82)

$$\frac{\partial^2\bar{\theta}(\lambda_n, x)}{\partial x^2} - \lambda_n^2\bar{\theta}(\lambda_n, x) = C_{2n} + \frac{1}{\gamma}\left(b_{1,n}e^{\mu_n x} + b_{2,n}e^{-\mu_n x}\right)$$

for 2L, 3L and 4 versions (83)

$$\frac{\partial^2\bar{\theta}(\lambda_n, x)}{\partial x^2} - \lambda_n^2\bar{\theta}(\lambda_n, x) = C_{3n} + \sum_{m=1}^{\infty} C_{3mn}\left(b_{1,m}e^{\mu_m x} + b_{2,m}e^{-\mu_m x}\right)$$

for 1L and 2C versions (84)

$$\frac{\partial^2\bar{\theta}(\lambda_n, y)}{\partial y^2} - \lambda_n^2\bar{\theta}(\lambda_n, y) = C_{4n} + \sum_{m=1}^{\infty} C_{4mn}\left(b_{1,m}e^{\mu_m y} + b_{2,m}e^{-\mu_m y}\right)$$

for 1S version (85)

where

$$C_{1n} = \sqrt{2}\frac{\lambda_n E_n}{1+\lambda_n^2}\left(\frac{\widehat{u}_s}{\gamma} - \widehat{T}_s\right) - \frac{b_{3,n}}{\gamma} \tag{86}$$

$$C_{2n} = \sqrt{\frac{2}{\gamma}}\frac{\lambda_n E_n}{1+\lambda_n^2}\left(\frac{\widehat{u}_s}{\gamma} - \widehat{T}_s\right) - \frac{b_{3,n}}{\gamma} \tag{87}$$

$$C_{3n} = \sqrt{\frac{2}{\gamma}}\frac{1}{\gamma}\frac{\widehat{u}_s}{1+e^{\gamma}}\frac{1}{1+\lambda_n^2}\left[\left(e^{\gamma}-1\right)(-1)^{n-1} + \left(e^{\gamma}+1\right)\lambda_n\right] - \frac{2}{\gamma}\frac{1}{\gamma}\sum_{m=1}^{\infty}(b_{3,m}I_{mn}) - \sqrt{\frac{2}{\gamma}}\frac{\widehat{T}_s\lambda_n}{1+\lambda_n^2} \tag{88}$$

$$C_{4n} = \sqrt{2}\frac{1}{\gamma}\frac{\widehat{u}_s}{1+e}\frac{1}{1+\lambda_n^2}\left[(e-1)(-1)^{n-1} + (e+1)\lambda_n\right] - 2\frac{1}{\gamma}\sum_{m=1}^{\infty}(b_{3,m}I_{mn}) - \sqrt{2}\frac{\widehat{T}_s\lambda_n}{1+\lambda_n^2} \tag{89}$$

$$C_{3mn} = \frac{2}{\gamma}\frac{I_{mn}}{\gamma} \tag{90}$$

$$C_{4mn} = 2\frac{I_{mn}}{\gamma} \tag{91}$$

$$I_{mn} = \frac{1}{2}(-1)^{m+n}\left[\frac{1}{(\mu_m - \lambda_n)} + \frac{1}{(\mu_m + \lambda_n)}\right] \tag{92}$$

A couple of the boundary conditions (Eqs. (74)–(77)) are used in the transformation process. Another couple that is not used is transformed in a similar manner as above and the ordinary differential equations are solved satisfying the transformed boundary conditions. The solution for each of the eight thermal versions are found as

$$\bar{\theta}_{2S}(\lambda_n, y) = c_{1,1}e^{\lambda_n y} + c_{1,2}e^{-\lambda_n y} + c_{1,3}ye^{\lambda_n y} + c_{1,4}ye^{-\lambda_n y} - c_{1,5} \tag{93}$$

$$\bar{\theta}_{3S}(\lambda_n, y) = c_{2,1}e^{\lambda_n y} + c_{2,2}e^{-\lambda_n y} + c_{2,3}ye^{\lambda_n y} + c_{2,4}ye^{-\lambda_n y} - c_{2,5} \tag{94}$$

$$\bar{\theta}_{2L}(\lambda_n, x) = c_{3,1}e^{\lambda_n x} + c_{3,2}e^{-\lambda_n x} + c_{3,3}xe^{\lambda_n x} + c_{3,4}xe^{-\lambda_n x} - c_{3,5} \tag{95}$$

$$\bar{\theta}_{3L}(\lambda_n, x) = c_{4,1}e^{\lambda_n x} + c_{4,2}e^{-\lambda_n x} + c_{4,3}xe^{\lambda_n x} + c_{4,4}xe^{-\lambda_n x} - c_{4,5} \tag{96}$$

$$\bar{\theta}_{4}(\lambda_n, x) = c_{5,1}e^{\lambda_n x} + c_{5,2}e^{-\lambda_n x} + c_{5,3}xe^{\lambda_n x} + c_{5,4}xe^{-\lambda_n x} - c_{5,5} \tag{97}$$

$$\bar{\theta}_{1L}(\lambda_n, x) = c_{6,1}e^{\lambda_n x} + c_{6,2}e^{-\lambda_n x} + \sum_{m=1}^{\infty}\left(c_{6,3}e^{\mu_m x} + c_{6,4}e^{-\mu_m x}\right) - c_{6,5} \tag{98}$$

$$\bar{\theta}_{2C}(\lambda_n, x) = c_{7,1}e^{\lambda_n x} + c_{7,2}e^{-\lambda_n x} + \sum_{m=1}^{\infty}\left(c_{7,3}e^{\mu_m x} + c_{7,4}e^{-\mu_m x}\right) - c_{7,5} \tag{99}$$

$$\bar{\theta}_{1S}(\lambda_n, y) = c_{8,1}e^{\lambda_n y} + c_{8,2}e^{-\lambda_n y} + \sum_{m=1}^{\infty}\left(c_{8,3}e^{\mu_m y} + c_{8,4}e^{-\mu_m y}\right) - c_{8,5} \tag{100}$$

The constant coefficients $c_{i,j}$ in the transformed functions above are given in Appendix A.

Applying the inversion formula for each of the transformed functions above and adding the appropriate auxiliary function result in the nondimensional temperature distribution as

$$\widehat{T}_{2S}(x, y) = \frac{\widehat{T}_s}{1+e}\left(e^{x} + e^{1-x}\right) + \sum_{n=1}^{\infty}K_{2S}(\lambda_n, x)\bar{\theta}_{2S}(\lambda_n, y) \tag{101}$$

$$\widehat{T}_{3S}(x,y)=\frac{\widehat{T}_s}{1+e}\left(e^{x}+e^{1-x}\right)+\sum_{n=1}^{\infty}K_{3S}(\lambda_n,x)\bar{\theta}_{3S}(\lambda_n,y) \tag{102}$$

$$\widehat{T}_{2L}(x,y)=\frac{\widehat{T}_s}{1+e^{\gamma}}\left(e^{y}+e^{\gamma-y}\right)+\sum_{n=1}^{\infty}K_{2L}(\lambda_n,y)\bar{\theta}_{2L}(\lambda_n,x) \tag{103}$$

$$\widehat{T}_{3L}(x,y)=\frac{\widehat{T}_s}{1+e^{\gamma}}\left(e^{y}+e^{\gamma-y}\right)+\sum_{n=1}^{\infty}K_{3L}(\lambda_n,y)\bar{\theta}_{3L}(\lambda_n,x) \tag{104}$$

$$\widehat{T}_{4}(x,y)=\frac{\widehat{T}_s}{1+e^{\gamma}}\left(e^{y}+e^{\gamma-y}\right)+\sum_{n=1}^{\infty}K_{4}(\lambda_n,y)\bar{\theta}_{4}(\lambda_n,x) \tag{105}$$

$$\widehat{T}_{1L}(x,y)=\frac{\widehat{T}_s}{e^{\gamma}+e^{-\gamma}}\left(e^{y-\gamma}+e^{\gamma-y}\right)+\sum_{n=1}^{\infty}K_{1L}(\lambda_n,y)\bar{\theta}_{1L}(\lambda_n,x) \tag{106}$$

$$\widehat{T}_{2C}(x,y)=\frac{\widehat{T}_s}{e^{\gamma}+e^{-\gamma}}\left(e^{y-\gamma}+e^{\gamma-y}\right)+\sum_{n=1}^{\infty}K_{2C}(\lambda_n,y)\bar{\theta}_{2C}(\lambda_n,x) \tag{107}$$

$$\widehat{T}_{1S}(x,y)=\frac{\widehat{T}_s}{e+e^{-1}}\left(e^{x-1}+e^{1-x}\right)+\sum_{n=1}^{\infty}K_{1S}(\lambda_n,x)\bar{\theta}_{1S}(\lambda_n,y) \tag{108}$$

The only unknown, nondimensional slip temperature $\widehat{T}_s$, may now be determined by nondimensionalizing Eq. (1) and adapting for the walls, which give the local nondimensional slip temperature at the walls as

$$\widehat{T}_s(x,0)=\widehat{T}_w+\frac{2R}{1+R}\frac{Kn}{Pr}\frac{2\gamma}{1+\gamma}\left.\frac{\partial\widehat{T}}{\partial y}\right|_{y=0}$$

$$\widehat{T}_s(x,\gamma)=\widehat{T}_w-\frac{2R}{1+R}\frac{Kn}{Pr}\frac{2\gamma}{1+\gamma}\left.\frac{\partial\widehat{T}}{\partial y}\right|_{y=\gamma}$$

$$\widehat{T}_s(0,y)=\widehat{T}_w+\frac{2R}{1+R}\frac{Kn}{Pr}\frac{2\gamma}{1+\gamma}\left.\frac{\partial\widehat{T}}{\partial x}\right|_{x=0}$$

$$\widehat{T}_s(1,y)=\widehat{T}_w-\frac{2R}{1+R}\frac{Kn}{Pr}\frac{2\gamma}{1+\gamma}\left.\frac{\partial\widehat{T}}{\partial x}\right|_{x=1} \tag{109}$$

Integrating the local nondimensional slip temperatures along the heated walls, and averaging over the nondimensional heated perimeter of microchannel gives the average nondimensional slip temperature $\widehat{T}_s$ as

$$\widehat{T}_s=\left[\int_0^{d_7}\widehat{T}_s(x,0)\,dx+\int_0^{d_{10}}\widehat{T}_s(x,\gamma)\,dx+\int_0^{d_1\gamma}\widehat{T}_s(0,y)\,dy+\int_0^{d_4\gamma}\widehat{T}_s(1,y)\,dy\right]\widehat{L}_h^{-1} \tag{110}$$

where the nondimensional heated perimeter of microchannel $\hat{L}_h$ for the eight thermal versions is calculated from

$$\hat{L}_h=L_h/a=d_7+d_{10}+d_1\gamma+d_4\gamma \tag{111}$$

Since partial derivative of the temperature with respect to x or y involves $\widehat{T}_s$ term, the equation above is implicit in $\widehat{T}_s$. Evaluating the integrals above and solving for the average nondimensional slip temperature $\widehat{T}_s$ result in its explicit form.

With the nondimensional velocity and temperature distributions and the nondimensional slip temperature known, the Nusselt number may now be determined. An energy balance on the heated perimeter at a specified ζ-cross section of microchannel leads to

$$q'd\zeta=hL_h\,d\zeta\,(T_w-T_b) \tag{112}$$

where the bulk or average nondimensional temperature $\widehat{T}_b$ is defined as

$$\widehat{T}_b=\frac{1}{\gamma}\int_0^{\gamma}\int_0^{1}\widehat{u}(x,y)\widehat{T}(x,y)\,dx\,dy \tag{113}$$

The Nusselt number is calculated by

$$Nu=\frac{hD_h}{k} \tag{114}$$

By combining Eq. (112) with Eq. (114) and after some manipulation the Nusselt number is found as

$$Nu=\frac{2\gamma}{1+\gamma}\frac{1}{\widehat{L}_h}\frac{1}{\widehat{T}_w-\widehat{T}_b} \tag{115}$$

8. Results and discussion

All the numerical calculations are done using Mathematica 5 package for $\widehat{T}_w=0$, $Pr=0.6$ and $R=1.4$. A sensitivity analysis on the number of terms in the infinite series is carried out to determine the required number of terms to be included in the infinite series to maintain a desired convergence and accuracy level. A typical Nusselt number calculation with varying number of terms in the infinite series for the 4 Version at $Kn=0.04$ and $\gamma=0.8$ is given in Fig. 2. The figure shows that the effect of the terms decreases rapidly and, disappears practically for the terms with $n>100$. The accuracy of the calculated Nusselt number, which is defined as the percentage of deviation from the converged value, for the number of terms equal to 100, 200 and 500 is as low as 0.025%, 0.013% and 0.006%, respectively. This allows calculating the infinite series with a relatively low number of terms (a few hundred terms) to provide the desired convergence and accuracy level. The very fast convergence of the series in the functions for velocity and temperature distributions makes the computer program time efficient.

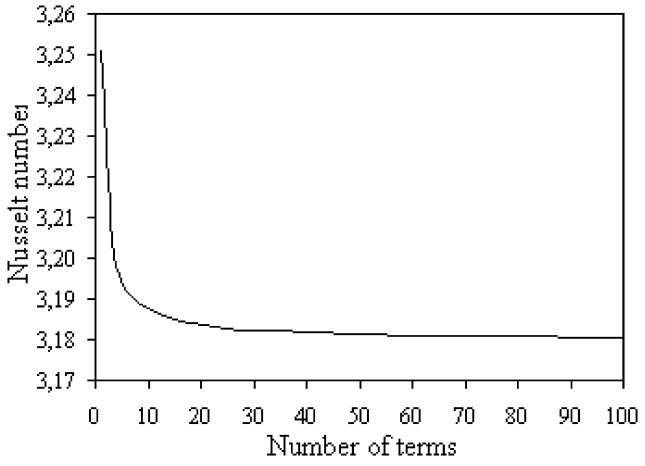

Fig. 2. Calculated Nusselt numbers with varying number of terms in the infinite series for the 4 version at $Kn = 0.04$ and $\gamma = 0.8$.

Table 3
Nusselt numbers for the 4 version

	$\gamma = 1$	$\gamma = 0.8$	$\gamma = 0.6$	$\gamma = 0.4$	$\gamma = 0.2$
Kn	*Nu*	*Nu*	*Nu*	*Nu*	*Nu*
0.00	3.6080	3.6638	3.8946	4.4719	5.7377
0.02	3.3812	3.4369	3.6337	4.0926	5.0087
0.04	3.1301	3.1797	3.3406	3.6970	4.3597
0.06	2.8848	2.9271	3.0569	3.3337	3.8219
0.08	2.6582	2.6935	2.7983	3.0154	3.3835
0.10	2.4540	2.4835	2.5686	2.7412	3.0253

Table 4
Nusselt numbers for the 3L version

	$\gamma = 1$	$\gamma = 0.8$	$\gamma = 0.6$	$\gamma = 0.4$	$\gamma = 0.2$
Kn	*Nu*	*Nu*	*Nu*	*Nu*	*Nu*
0.00	3.5682	3.8358	4.2464	4.9233	6.1311
0.02	3.2994	3.5286	3.8692	4.3998	5.2601
0.04	3.0306	3.2219	3.4979	3.9079	4.5252
0.06	2.7812	2.9398	3.1629	3.4817	3.9353
0.08	2.5574	2.6891	2.8706	3.1219	3.4642
0.10	2.3592	2.4694	2.6186	2.8198	3.0847

The Nusselt numbers calculated for the eight thermal versions are given in Tables 3–10 as a function of aspect ratio γ and Knudsen number *Kn*. The Nusselt numbers for non-slip flow in macrochannels for all the eight thermal versions are determined by setting $Kn = 0$. The first lines on the Tables 3–10 correspond to this case. The Nusselt numbers for non-slip flow in macrochannels found by Morini [1] and Shah and London [13] are given in Tables 11 and 12, respectively. A comparison between the data on the first lines of the Tables 3–10 and the data given in the Tables 11 and 12 shows that the Nusselt numbers found for non-slip flow in macrochannels in this paper are in exact agreement with those of Morini [1] and good agreement with those of Shah and London [13]. On the other hand, Yu and Ameel [5] solved slip flow in microchannels for 4 version for thermally developing flow. Since the results found by Yu and Ameel [5] are given for thermally developing flow and in graphical form, a precise comparison between the results is not possible. However, a qualitative comparison shows that the

Table 5
Nusselt numbers for the 2L version

	$\gamma = 1$	$\gamma = 0.8$	$\gamma = 0.6$	$\gamma = 0.4$	$\gamma = 0.2$
Kn	*Nu*	*Nu*	*Nu*	*Nu*	*Nu*
0.00	4.0950	4.4717	4.9440	5.5924	6.6089
0.02	3.6802	3.9842	4.3585	4.8511	5.5596
0.04	3.3101	3.5536	3.8472	4.2194	4.7209
0.06	2.9906	3.1866	3.4185	3.7035	4.0691
0.08	2.7173	2.8769	3.0625	3.2849	3.5596
0.10	2.4838	2.6153	2.7661	2.9430	3.1553

Table 6
Nusselt numbers for the 1L version

	$\gamma = 1$	$\gamma = 0.8$	$\gamma = 0.6$	$\gamma = 0.4$	$\gamma = 0.2$
Kn	*Nu*	*Nu*	*Nu*	*Nu*	*Nu*
0.00	2.6855	2.9644	3.3086	3.7503	4.3784
0.02	2.4661	2.7003	2.9852	3.3432	3.8276
0.04	2.2723	2.4699	2.7066	2.9978	3.3766
0.06	2.1026	2.2704	2.4688	2.7083	3.0101
0.08	1.9539	2.0977	2.2656	2.4650	2.7100
0.10	1.8232	1.9476	2.0911	2.2592	2.4615

Table 7
Nusselt numbers for the 3S version

	$\gamma = 1$	$\gamma = 0.8$	$\gamma = 0.6$	$\gamma = 0.4$	$\gamma = 0.2$
Kn	*Nu*	*Nu*	*Nu*	*Nu*	*Nu*
0.00	3.5682	3.3553	3.1818	3.1631	3.6387
0.02	3.2994	3.1274	2.9836	2.9609	3.3183
0.04	3.0306	2.8905	2.7702	2.7444	3.0140
0.06	2.7812	2.6658	2.5642	2.5371	2.7433
0.08	2.5574	2.4611	2.3746	2.3474	2.5078
0.10	2.3592	2.2781	2.2037	2.1773	2.3043

Table 8
Nusselt numbers for the 2S version

	$\gamma = 1$	$\gamma = 0.8$	$\gamma = 0.6$	$\gamma = 0.4$	$\gamma = 0.2$
Kn	*Nu*	*Nu*	*Nu*	*Nu*	*Nu*
0.00	4.0950	3.7129	3.2260	2.5829	1.6586
0.02	3.6802	3.3800	2.9847	2.4382	1.6040
0.04	3.3102	3.0714	2.7485	2.2850	1.5396
0.06	2.9906	2.7979	2.5315	2.1369	1.4729
0.08	2.7174	2.5595	2.3372	1.9993	1.4073
0.10	2.4840	2.3527	2.1652	1.8736	1.3446

Nusselt numbers found for the 4 version at slip condition in this paper (the data on Table 3) are in good agreement with those of Yu and Ameel [5]. Note that the Nusselt numbers found for the 3L and 3S, 2L and 2S, 1L and 1S, versions are equal at $\gamma = 1$, which is an expected situation. The numerical results also show that, for a given aspect ratio and rarefaction, the heat transfer in the 2L version is higher than that for all the other thermal versions. The highest heat transfer is achieved in the 2L version with the smallest aspect ratio. For macrochannels under H1 [1] or H2 [2] boundary conditions also, the highest heat transfer is observed in the 2L version. This is justified by Spiga and Morini [14] that among the eight thermal versions, as the aspect ratio approaches zero only the 2L version approaches the slab geometry having the well-known Nusselt number as high

Table 9
Nusselt numbers for the 1S version

	$\gamma = 1$	$\gamma = 0.8$	$\gamma = 0.6$	$\gamma = 0.4$	$\gamma = 0.2$
Kn	*Nu*	*Nu*	*Nu*	*Nu*	*Nu*
0.00	2.6855	2.4036	2.0476	1.5846	0.9511
0.02	2.4661	2.2286	1.9219	1.5106	0.9250
0.04	2.2723	2.0704	1.8046	1.4385	0.8980
0.06	2.1025	1.9293	1.6973	1.3703	0.8713
0.08	1.9538	1.8038	1.6000	1.3067	0.8453
0.10	1.8231	1.6922	1.5119	1.2476	0.8204

Table 10
Nusselt numbers for the 2C version

	$\gamma = 1$	$\gamma = 0.8$	$\gamma = 0.6$	$\gamma = 0.4$	$\gamma = 0.2$
Kn	*Nu*	*Nu*	*Nu*	*Nu*	*Nu*
0.00	2.8108	2.8405	2.9613	3.2563	3.9246
0.02	2.6066	2.6351	2.7407	2.9879	3.5115
0.04	2.4138	2.4395	2.5297	2.7350	3.1482
0.06	2.2383	2.2607	2.3375	2.5084	2.8393
0.08	2.0810	2.1004	2.1659	2.3092	2.5786
0.10	1.9407	1.9576	2.0137	2.135	2.3577

Table 11
Nusselt numbers for non-slip flow found by Morini [1]

	Morini [1]				
	$\gamma = 1$	$\gamma = 0.8$	$\gamma = 0.6$	$\gamma = 0.4$	$\gamma = 0.2$
	Nu	*Nu*	*Nu*	*Nu*	*Nu*
4 version	3.608	3.664	3.895	4.472	5.738
3L version	3.568	3.836	4.246	4.923	6.131
2L version	4.095	4.472	4.944	5.592	6.609
1L version	2.686	2.964	3.309	3.750	4.379
3S version	3.568	3.355	3.182	3.163	3.639
2S version	4.095	3.713	3.226	2.583	1.659
1S version	2.686	2.404	2.048	1.585	0.951
2C version	2.811	2.840	2.961	3.256	3.925

Table 12
Nusselt numbers for non-slip flow found by Shah and London [13]

	Shah and London [13]				
	$\gamma = 1$	$\gamma = 0.8$	$\gamma = 0.6$	$\gamma = 0.4$	$\gamma = 0.2$
	Nu	*Nu*	*Nu*	*Nu*	*Nu*
4 version	3.608	3.664	3.895	4.472	5.738
3L version	3.556	–	–	4.885	6.072
2L version	4.094	–	–	5.555	6.561
1L version	2.712	–	–	3.777	4.411
3S version	3.556	–	–	3.169	3.636
2S version	4.094	–	–	2.598	1.664
1S version	2.712	–	–	1.604	0.964
2C version	2.836	2.866	2.987	3.279	3.914

as 8.235. For each of the thermal versions, a Nusselt number correlation in terms of aspect ratio and Knudsen number can be given by making use of the numerical values on Tables 3–10 for the purpose of practical usages.

The numerical data on Tables 3–10 shows that Nusselt number for a microchannel with any aspect ratio decreases as the Knudsen number increases for all the thermal versions. This means that, with no exception, rarefaction influences the heat transfer in negative direction. The higher the rarefaction, the lower the heat transfer. From geometrical point of view, this simply means that as the characteristic size of a microchannel decreases, the heat transfer decreases also. Typical variation of heat transfer with rarefaction, for the 4 version, is given in Fig. 3.

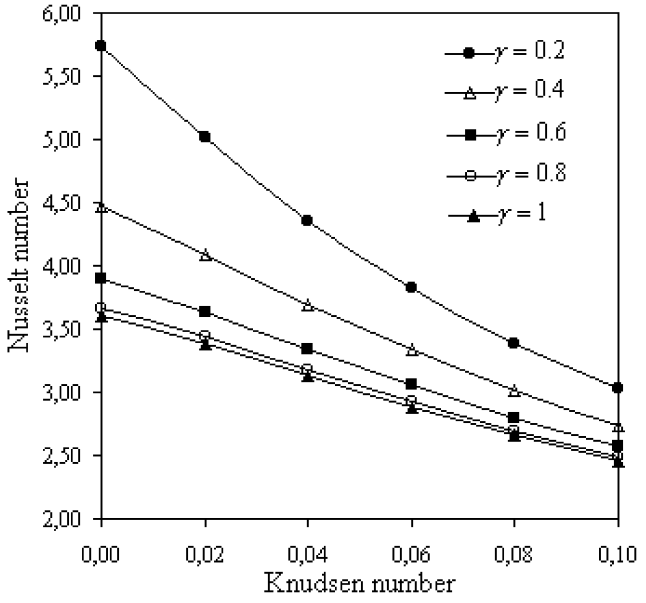

Fig. 3. Variation of Nusselt number with Knudsen number for the 4 version.

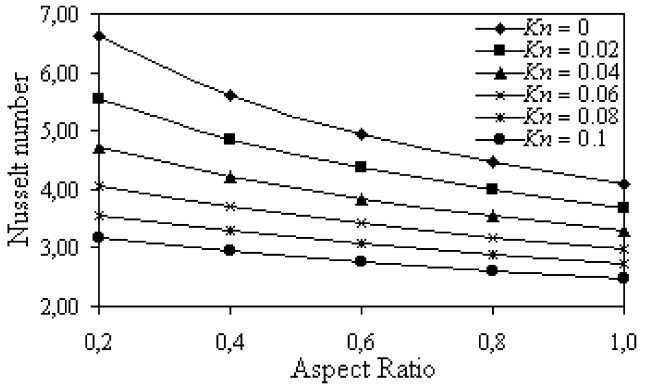

Fig. 4. Variation of Nusselt number with aspect ratio for the 2L version.

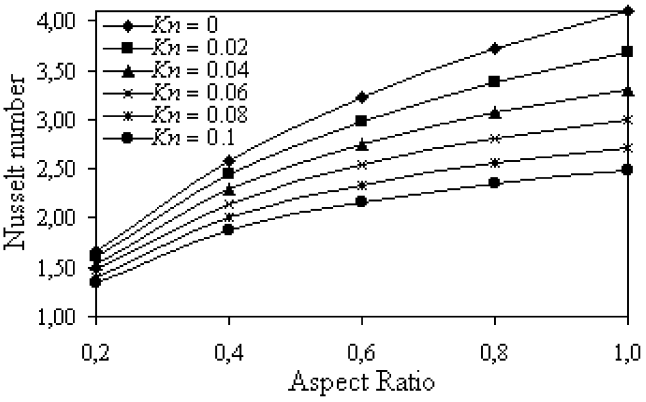

Fig. 5. Variation of Nusselt number with aspect ratio for the 2S version.

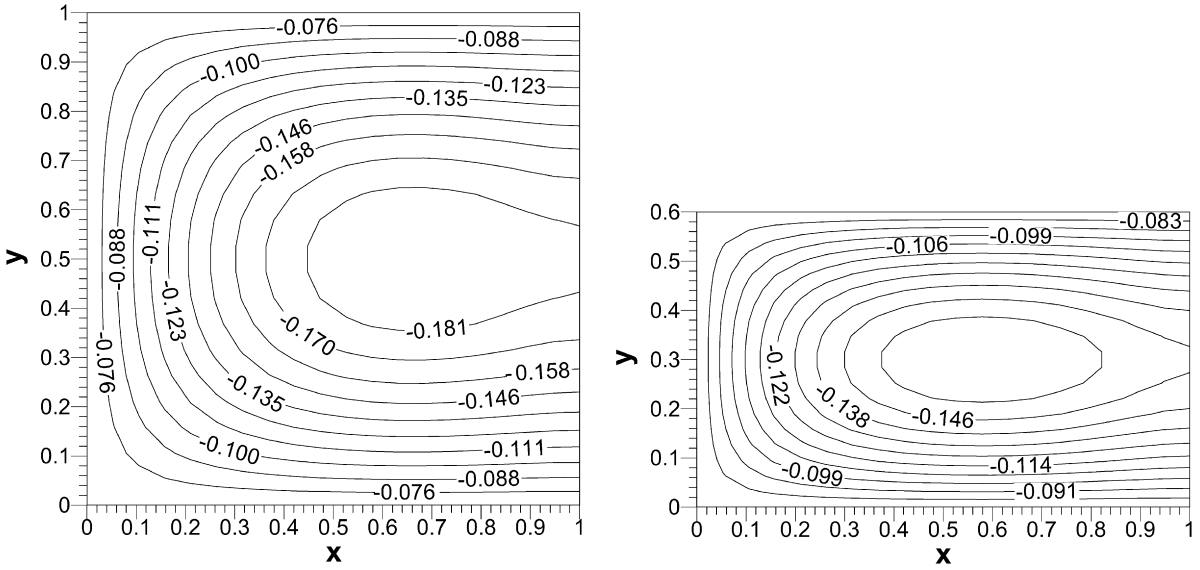

Fig. 6. Temperature contours for the 3L thermal version for $\gamma = 1$ and $\gamma = 0.6$.

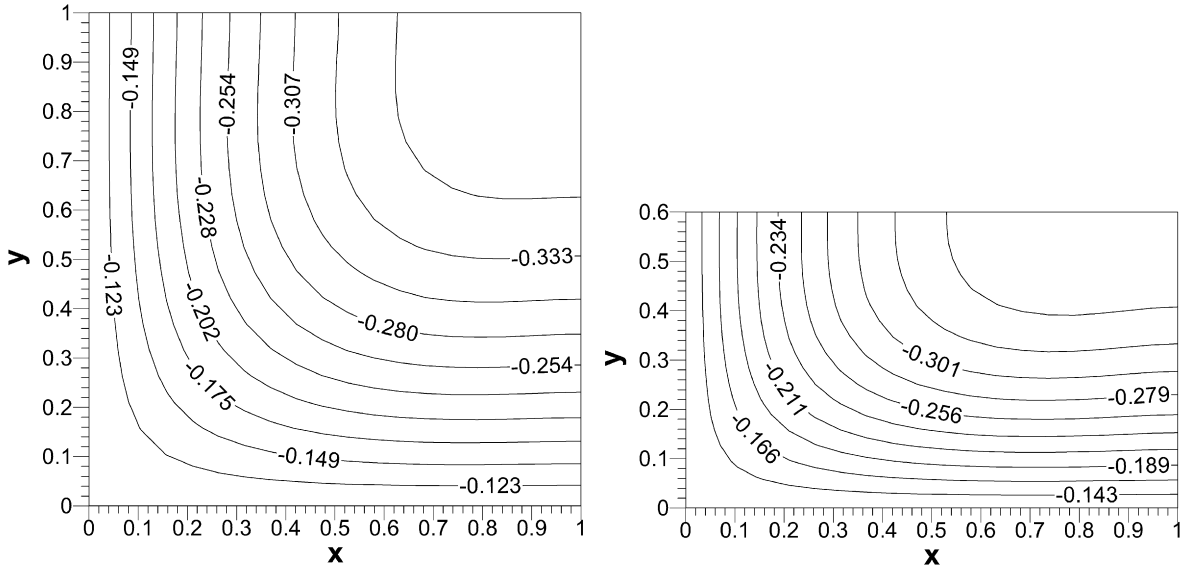

Fig. 7. Temperature contours for the 2C thermal version for $\gamma = 1$ and $\gamma = 0.6$.

The effect of aspect ratio on heat transfer is not similar to that of the rarefaction. Heat transfer decreases for the 4, 3L, 2L, 1L and 2C versions and, increases for the 3S, 2S and 1S versions, with increasing aspect ratio, with an exception for the 3S version at very low aspect ratios, that exhibits a decreasing trend. In other words, the highest heat transfer for the 4, 3L, 2L, 1L and 2C versions is achieved at the lowest aspect ratio while, the highest heat transfer for the 3S, 2S and 1S versions is achieved at the highest aspect ratio ($\gamma = 1$). A typical variation of the heat transfer with aspect ratio for the 2L and 2S versions are given in Figs. 4 and 5, respectively. The figures show that the rate of decrease or increase with aspect ratio slows down at high rarefactions. This holds for all the thermal versions. Further, the numerical data for the 4 and 2C versions shows that the change in Nusselt number for different high aspect ratios is very small. Therefore, the effect of aspect ratio on heat transfer for the 4 and 2C versions can be neglected at high aspect ratios with high accuracy.

The temperature contours for the 3L and 2C thermal versions are given in Figs. 6 and 7, respectively. The temperature contours for each thermal version are plotted typically for aspect ratios equal to 0.6 and 1. Note that the temperature contours plotted in microchannels with aspect ratio equal to 1 for the 3L and 3S, 2L and 2S, 1L and 1S, versions are identical with ninety degrees geometrical rotation, as expected. The figures show that the hottest and coldest contour lines are located closest and farthest to the heated walls, respectively. Finally, it is notable that the numerical data of Tables 3–10 and the temperature contours may be used to determine the optimal geometrical and operational conditions for a microchannel exposed to any of the eight thermal versions.

9. Conclusion

Thermal behavior of a hydrodynamically and thermally developed flow in rectangular microchannels is analyzed. The continuum approach with the velocity slip and temperature jump condition at the solid walls is applied to develop the mathematical model of flow phenomenon in the rectangular microchannel. A total of eight different thermal boundary conditions that are formed of different combinations of heated (at constant temperature) and adiabatic walls is considered. The solution of mathematical model is achieved by applying integral transform method to both the momentum and energy equations. The velocity and temperature distributions found by the solution of the momentum and energy equations are used to determine the average Nusselt number for all the eight thermal versions. The solution method of the paper is validated for all the eight thermal versions at non-slip flow condition, and for a single thermal version (4 version) at slip flow condition. The paper explores the effects of rarefaction and aspect ratio on thermal character of flow in rectangular microchannels exposed to the eight different thermal boundary conditions. The study does not include the effect of tangential momentum accommodation coefficient and thermal accommodation coefficient. Numerical results are obtained for the fixed values of physical properties ($Pr = 0.6$, $R = 1.4$) and wall temperature ($\widehat{T}_w = 0$). The results show that the highest heat transfer is achieved in the microchannel with two heated long walls (at constant temperature) and two adiabatic short walls (2L version). The decreasing effect of rarefaction on heat transfer in microchannels, for all the thermal versions, is established. The higher the rarefaction, the lower the heat transfer. The numerical results also show that heat transfer for the eight thermal versions may increase, decrease, or exhibit very small change with aspect ratio. In particular, heat transfer decreases for the 4, 3L, 2L, 1L and 2C versions, and increases for the 3S, 2S and 1S versions with increasing aspect ratio. The rate of change in heat transfer for the 4 and 2C versions at high aspect ratios is very small. Therefore, the effect of aspect ratio on heat transfer for the 4 and 2C versions can be neglected at high aspect ratios with high accuracy. The solution of the paper may be used to determine the optimal geometrical and operational conditions for a microchannel exposed to any of the eight thermal versions.

Appendix A

The constant coefficients $c_{i,j}$ in the transformed functions, Eqs. (93)–(100), are given as

$$c_{1,1} = -\frac{c_{1,3}}{\lambda_n} - \frac{\gamma(c_{1,3}e^{\lambda_n\gamma} - c_{1,4}e^{-\lambda_n\gamma})}{e^{\lambda_n\gamma} - e^{-\lambda_n\gamma}} \tag{A.1}$$

$$c_{1,2} = \frac{c_{1,4}}{\lambda_n} - \frac{\gamma(c_{1,3}e^{\lambda_n\gamma} - c_{1,4}e^{-\lambda_n\gamma})}{e^{\lambda_n\gamma} - e^{-\lambda_n\gamma}} \tag{A.2}$$

$$c_{1,3} = c_{2,3} = c_{3,3} = c_{4,3} = c_{5,3} = \frac{b_{1,n}}{2\gamma\lambda_n} \tag{A.3}$$

$$c_{1,4} = c_{2,4} = c_{3,4} = c_{4,4} = c_{5,4} = -\frac{b_{2,n}}{2\gamma\lambda_n} \tag{A.4}$$

$$c_{1,5} = c_{2,5} = \frac{C_{1n}}{\lambda_n^2} \tag{A.5}$$

$$c_{2,1} = \frac{D_{2,n}e^{-\lambda_n\gamma}}{(e^{\lambda_n\gamma} + e^{-\lambda_n\gamma})} - \frac{c_{2,3}e^{\lambda_n\gamma}(1+\lambda_n\gamma) + c_{2,4}e^{-\lambda_n\gamma}(1-\lambda_n\gamma)}{\lambda_n(e^{\lambda_n\gamma} + e^{-\lambda_n\gamma})} \tag{A.6}$$

$$c_{2,2} = \frac{D_{2,n}e^{\lambda_n\gamma}}{(e^{\lambda_n\gamma} + e^{-\lambda_n\gamma})} + \frac{c_{2,3}e^{\lambda_n\gamma}(1+\lambda_n\gamma) + c_{2,4}e^{-\lambda_n\gamma}(1-\lambda_n\gamma)}{\lambda_n(e^{\lambda_n\gamma} + e^{-\lambda_n\gamma})} \tag{A.7}$$

$$D_{2,n} = \sqrt{2}\frac{E_n}{\gamma\lambda_n^3}\left(\widehat{u}_s - \frac{P}{\lambda_n^2}\right) \tag{A.8}$$

$$c_{3,1} = -\frac{c_{3,3}}{\lambda_n} - \frac{c_{3,3}e^{\lambda_n} - c_{3,4}e^{-\lambda_n}}{e^{\lambda_n} - e^{-\lambda_n}} \tag{A.9}$$

$$c_{3,2} = \frac{c_{3,4}}{\lambda_n} - \frac{c_{3,3}e^{\lambda_n} - c_{3,4}e^{-\lambda_n}}{e^{\lambda_n} - e^{-\lambda_n}} \tag{A.10}$$

$$c_{3,5} = c_{4,5} = c_{5,5} = \frac{C_{2n}}{\lambda_n^2} \tag{A.11}$$

$$c_{4,1} = \frac{D_{4,n}e^{-\lambda_n}}{(e^{\lambda_n} + e^{-\lambda_n})} - \frac{c_{4,3}e^{\lambda_n}(1+\lambda_n) + c_{4,4}e^{-\lambda_n}(1-\lambda_n)}{\lambda_n(e^{\lambda_n} + e^{-\lambda_n})} \tag{A.12}$$

$$c_{4,2} = \frac{D_{4,n}e^{\lambda_n}}{(e^{\lambda_n} + e^{-\lambda_n})} + \frac{c_{4,3}e^{\lambda_n}(1+\lambda_n) + c_{4,4}e^{-\lambda_n}(1-\lambda_n)}{\lambda_n(e^{\lambda_n} + e^{-\lambda_n})} \tag{A.13}$$

$$D_{4,n} = D_{5,n} = \sqrt{\frac{2}{\gamma}}\frac{E_n}{\gamma\lambda_n^3}\left(\widehat{u}_s - \frac{P}{\lambda_n^2}\right) \tag{A.14}$$

$$c_{5,1} = \frac{-D_{5,n}e^{-\lambda_n} - c_{5,3}e^{\lambda_n} - c_{5,4}e^{-\lambda_n} + D_{5,n}}{e^{\lambda_n} - e^{-\lambda_n}} \tag{A.15}$$

$$c_{5,2} = \frac{D_{5,n}e^{\lambda_n} + c_{5,3}e^{\lambda_n} + c_{5,4}e^{-\lambda_n} - D_{5,n}}{e^{\lambda_n} - e^{-\lambda_n}} \tag{A.16}$$

$$c_{6,1} = \frac{1}{\lambda_n(e^{\lambda_n} - e^{-\lambda_n})}\left[e^{-\lambda_n}\sum_{m=1}^{\infty}(c_{6,3}\mu_m - c_{6,4}\mu_m) - \sum_{m=1}^{\infty}\left(c_{6,3}\mu_m e^{\mu_m} - c_{6,4}\mu_m e^{-\mu_m}\right)\right] \tag{A.17}$$

$$c_{6,2} = \frac{1}{\lambda_n(e^{\lambda_n} - e^{-\lambda_n})}\left[e^{\lambda_n}\sum_{m=1}^{\infty}(c_{6,3}\mu_m - c_{6,4}\mu_m) - \sum_{m=1}^{\infty}\left(c_{6,3}\mu_m e^{\mu_m} - c_{6,4}\mu_m e^{-\mu_m}\right)\right] \tag{A.18}$$

$$c_{6,3} = c_{7,3} = \frac{C_{3mn}b_{1,m}}{\mu_m^2 - \lambda_n^2} \tag{A.19}$$

$$c_{6,4} = c_{7,4} = \frac{C_{3mn}b_{2,m}}{\mu_m^2 - \lambda_n^2} \tag{A.20}$$

$$c_{6,5} = c_{7,5} = \frac{C_{3n}}{\lambda_n^2} \tag{A.21}$$

$$c_{7,1} = \frac{e^{-\lambda_n}}{(e^{\lambda_n} + e^{-\lambda_n})}\left[D_{7,n} - \sum_{m=1}^{\infty}(c_{7,3} + c_{7,4}) \right] - \frac{1}{\lambda_n(e^{\lambda_n} + e^{-\lambda_n})} \sum_{m=1}^{\infty} \mu_m \left(c_{7,3} e^{\mu_m} - c_{7,4} e^{-\mu_m} \right) \quad \text{(A.22)}$$

$$c_{7,2} = \frac{e^{\lambda_n}}{(e^{\lambda_n} + e^{-\lambda_n})}\left[D_{7,n} - \sum_{m=1}^{\infty}(c_{7,3} + c_{7,4}) \right] + \frac{1}{\lambda_n(e^{\lambda_n} + e^{-\lambda_n})} \sum_{m=1}^{\infty} \mu_m \left(c_{7,3} e^{\mu_m} - c_{7,4} e^{-\mu_m} \right) \quad \text{(A.23)}$$

$$D_{7,n} = \sqrt{\frac{2}{\gamma}} \frac{\widehat{T}_s}{\lambda_n(1 + \lambda_n^2)} + \frac{C_n}{\lambda_n^2} \quad \text{(A.24)}$$

$$c_{8,1} = \frac{1}{\lambda_n(e^{\lambda_n \gamma} - e^{-\lambda_n \gamma})}\left[e^{-\lambda_n \gamma} \sum_{m=1}^{\infty}(c_{8,3}\mu_m - c_{8,4}\mu_m) - \sum_{m=1}^{\infty}\left(c_{8,3}\mu_m e^{\mu_m \gamma} - c_{8,4}\mu_m e^{-\mu_m \gamma} \right) \right] \quad \text{(A.25)}$$

$$c_{8,2} = \frac{1}{\lambda_n(e^{\lambda_n \gamma} - e^{-\lambda_n \gamma})}\left[e^{\lambda_n \gamma} \sum_{m=1}^{\infty}(c_{8,3}\mu_m - c_{8,4}\mu_m) - \sum_{m=1}^{\infty}\left(c_{8,3}\mu_m e^{\mu_m \gamma} - c_{8,4}\mu_m e^{-\mu_m \gamma} \right) \right] \quad \text{(A.26)}$$

$$c_{8,3} = \frac{C_{4mn} b_{1,m}}{\mu_m^2 - \lambda_n^2} \quad \text{(A.27)}$$

$$c_{8,4} = \frac{C_{4mn} b_{2,m}}{\mu_m^2 - \lambda_n^2} \quad \text{(A.28)}$$

$$c_{8,5} = \frac{C_{4n}}{\lambda_n^2} \quad \text{(A.29)}$$

References

[1] G.L. Morini, Analytical determination of the temperature distribution and Nusselt numbers in rectangular ducts with constant axial heat flux, International Journal of Heat and Mass Transfer 43 (5) (2000) 741–755.

[2] M. Spiga, G.L. Morini, Nusselt numbers in laminar flow for H2 boundary conditions, International Journal of Heat and Mass Transfer 39 (6) (1996) 1165–1174.

[3] G. Tunc, Y. Bayazitoglu, Heat transfer in rectangular microchannels, International Journal of Heat and Mass Transfer 45 (4) (2002) 765–773.

[4] L. Ghodoossi, N. Egrican, Prediction of heat transfer characteristics in rectangular microchannels for slip flow regime and H1 boundary condition, International Journal of Thermal Sciences 44 (6) (2005) 513–520.

[5] S. Yu, T.A. Ameel, Slip-flow heat transfer in rectangular microchannels, International Journal of Heat and Mass Transfer 44 (22) (2001) 4225–4234.

[6] A. Beskok, G.E. Karniadakis, Simulation of slip-flows in complex microgeometries, in: Micromechanical Systems. Book No. G00783-1992, in: ASME DSC, vol. 40, 1992, pp. 355–370.

[7] R.F. Barron, X. Wang, T.A. Ameel, R.O. Warrington, The Graetz problem extended to slip-flow, International Journal of Heat and Mass Transfer 40 (8) (1997) 1817–1823.

[8] M.N. Ozisik, Boundary Value Problems of Heat Conduction, International Textbook Company, Scranton, Pennsylvania, 1968.

[9] M.N. Ozisik, Heat Conduction, second ed., John Wiley & Sons, New York, 1993.

[10] R.M. Cotta, Integral Transforms in Computational Heat and Fluid Flow, CRC Press, Boca Raton, FL, 1993.

[11] R.M. Cotta, The Integral Transform Method in Thermal and Fluids Sciences and Engineering, Begell House, New York, 1998.

[12] B. Davies, Integral Transforms and Their Applications, third ed., Springer, Berlin, 2002.

[13] R.K. Shah, A.L. London, Laminar flow forced convection in ducts, Adv. Heat Transfer 14 (1978).

[14] M. Spiga, G.L. Morini, Laminar heat transfer between parallel plates as the limiting solution for the rectangular duct, International Communications in Heat and Mass Transfer 23 (4) (1996) 555–562.